Fizika Nizkikh Temperatur, 2011, v. 37, No. 2, p. 161–166

Evidence for non-Dzyaloshinskii–Moriya ferromagnetism in epitaxial $BiFeO_3$ films

V.G. Prokhorov and G.G. Kaminsky

Institute of Metal Physics, NASU, Kiev, 03142 Ukraine
E-mail: pvg@imp.kiev.ua

J.M. Kim, T.W. Eom, J.S. Park, and Y.P. Lee

q-Psi and Department of Physics, Hanyang University, Seoul, 133-791 Korea

V.L. Svetchnikov

National Center for HREM, TU Delft, 2628AL The Netherlands

G.G. Levtchenko, Yu.M. Nikolaenko, and V.A. Khokhlov

Donetsk Institute for Physics and Technology, NASU, Donetsk, 83114 Ukraine

Received May 26, 2010

$BiFeO_3$ films have been prepared by dc magnetron sputtering on $LaAlO_3$ (001) single-crystalline substrate. X-ray diffraction analysis and high-resolution electron-microscopy study reveal that the films have a highly *c*-oriented orthorhombic crystal structure. It was found that the magnetic properties of the $BiFeO_3$ films are typical for the ensemble of interacting superparamagnetic clusters rather than for the Dzyaloshinskii–Moriya weak ferromagnet. Appearance of the *extrinsic* nanoscale superparamagnetic clusters is explained by the oxygen deficiency in certain regions of the film, where the ferromagnetic ordering is realized through the double-exchange mechanism by Zener.

PACS: 75.50.Bb Fe and its alloys;
75.50.Ee Antiferromagnetics;
75.60.Ej Magnetization curves, hysteresis, Barkhausen and related effects;
77.55.Nv Multiferroic/magnetoelectric films.

Keywords: multiferroics, Dzyaloshinskii–Moriya ferromagnetism, superparamagnetic clusters.

1. Introduction

Multiferroics have attracted considerable attention due to their interesting fundamental science, connected with simultaneous effects of ferroelectric and magnetic order, and potential for applications in information storage, such as spintronic devices and sensors. The perovskite $BiFeO_3$ is a typical multiferroic compound with ferroelectric transition temperature $T_C \simeq 1103$ K and antiferromagnetic (AFM) transition $T_N \simeq 643$ K [1–3]. The bulk single crystal has a rhombohedral crystal lattice with unit-cell parameters $a_R \simeq 0.563$ nm and $\alpha_R \simeq 59.4$ [4,5]. In spite of room temperature multiferroicity, bulk $BiFeO_3$ is a canted *G*-type AFM with a weak ferromagnetic (FM) moment ($\simeq 0.02\ \mu_B$/Fe) [6], which arise from the antisymmetric Dzyaloshinskii–Moriya (DM) exchange [7–9]. At the same time, the enhancement in FM response of $BiFeO_3$ assumes importance because such improvement can help in utilizing of this compound for practical applications. Recently, enhanced ferroelectric properties (including the FM magnetic moment) have been observed in $BiFeO_3$ thin films, deposited on the single-crystalline substrates [5,10–12]. The slight enhancement of FM-like magnetic moment is attributed to the oxygen deficiencies [5] and the lattice strains [12], accumulated during an epitaxial film growth. The main explanation of this effect is based on suppression of helical AFM order, which can lead to enhancement of the DM interaction and give rise to higher FM magnetic moment. However, the additional extrinsic factors can be play

important role in formation of the FM state in the epitaxial $BiFeO_3$ films [13].

In this paper we report the experimental results for $BiFeO_3$ (BFO) films deposited on $LaAlO_3$ (LAO) (001) single-crystalline substrates. The observed evidence for the non-DM-like FM response is discussed in detail.

2. Experimental techniques

The films were prepared by dc magnetron sputtering at a substrate temperature of 650 °C [14]. To avoid the influence of lattice strain, accumulated during deposition, the all films were annealed at 900 °C for 2 h in air. The thickness of the films was $d \simeq 150$ nm. The θ–2θ x-ray diffraction (XRD) patterns were obtained using a Rigaku diffractometer with Cu K_α radiation. The high-resolution electron-microscopy (HREM) study was carried out using a Philips CM300UT-FEG microscope with a field emission gun operated at 300 kV. The point resolution of the microscope was in the order of 0.12 nm. All microstructure measurements were carried out at room temperature. The field-cooled (FC) and the zero-field-cooled (ZFC) magnetization curves were taken with a Quantum Design SQUID magnetometer for the in-plane magnetic field orientation. To avoid the influence of diamagnetic response from LAO, the magnetization curves obtained for the bare substrates were extracted from the raw experimental curves.

3. Microstructure of films

Figure 1 presents (*a*) the XRD pattern and (*b*) the cross-sectional high-magnification HREM image taken from the [010] zone axis for BFO, including the film/substrate interface. The θ–2θ XRD scan for the film displays only the fundamental Bragg peaks for the film and the substrate, indicating that the deposition results in a highly *c*-oriented crystal structure. It is seen that the film manifests the atomically clean and sharp interface without an amorphous intermediate layer or precipitations. The epitaxial relationship for film and substrate is determined to be $[001]_{BFO} \| [001]_{LAO}$. It is confirmed by the corresponding fast Fourier transform (FFT) for the HREM image, represented by inset in Fig. 1,*b*, which reveals the almost rectangular pattern only of basic Bragg spots. The slight splitting of Bragg spots (indicated by two short arrows) is connected with the difference between film and substrate crystal lattice. According to a microstructure analysis, the prepared films have the orthorhombic crystal structure with lattice parameters $a \simeq b \simeq 0.3997$ nm, $c \simeq 0.4045$ nm, and angle between atomic rows $\theta \simeq 89.4°$ that is well coincident with the published results [5,10–12].

4. Magnetic properties

Figure 2 shows the in-plane FC (solid symbols) and the ZFC (open symbols) temperature dependences of the magnetic moment, $M(T)$, taken at different applied magnetic fields, after an extracting of diamagnetic response from the substrate. For comparison, inset displays the raw FC $M(T)$ curves for the substrate with (solid symbols) and without (open symbols) deposited film. In both cases the LAO size was the same, $0.5 \times 0.5 \times 0.5$ mm. It is seen that the $M(T)$ dependences for bare LAO substrate manifest a nonlinear behavior with a well-defined increase of magnetic moment in the low-temperature range. Such exponential rise of $M(T)$ with decreasing temperature can be explained by a presence of paramagnetic impurities in the LAO substrate. Therefore, the additional $M(T)$ measurements of a bare substrate are very important for a correct interpretation of magnetic properties of the BFO film.

The $M(T)$ behavior shown by Fig. 2 is typical for a multiphase magnetic system, involving the AFM matrix

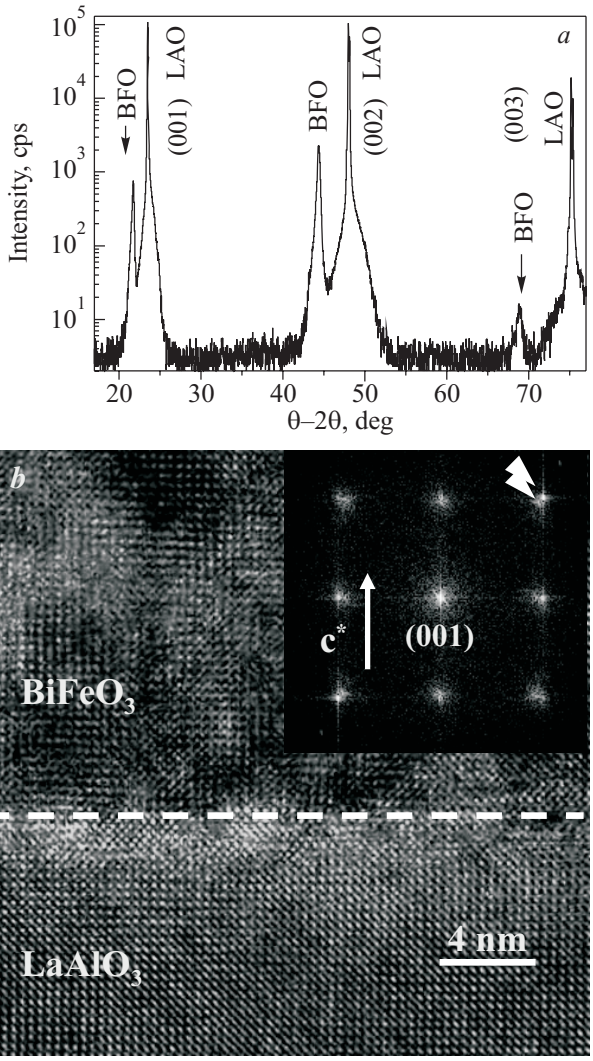

Fig. 1. (*a*) XRD scan for BFO/LAO film. Only fundamental Bragg peaks for the film (BFO) and the substrate (LAO) are recognized. (*b*) High-magnification cross-sectional HREM image taken at the BFO/LAO interface. The dashed line indicates the interface. Inset shows FFT of the same HREM image.

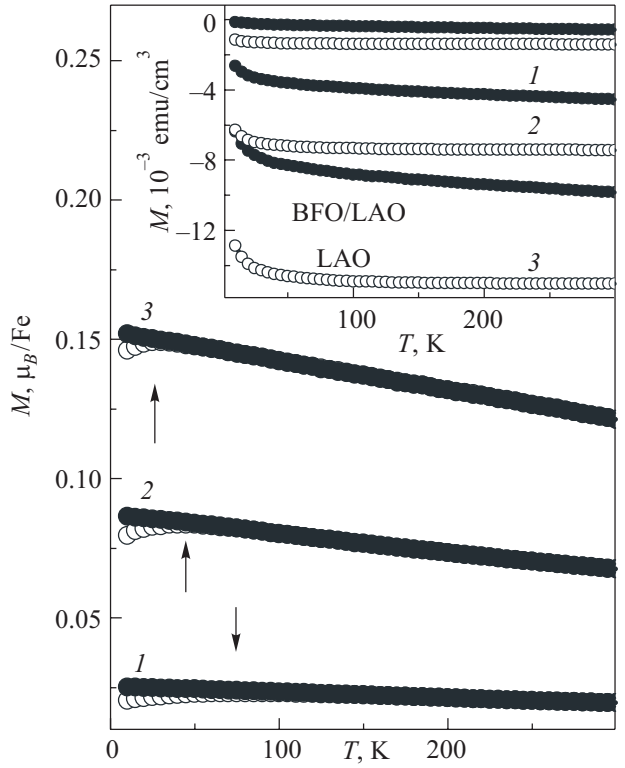

Fig. 2. Temperature dependence of the in-plane ZFC (open symbols) and FC (solid symbols) magnetic moment for the BFO film (after extracting of the substrate response), measured in an applied magnetic field of 0.1 (*1*), 0.5 (*2*), and 1.0 (*3*) T. Arrows indicate the temperature of ZFC/FC $M(T)$ splitting. Inset shows the raw in-plane FC $M(T)$ dependencies for the film with substrate (BFO/LAO, solid symbols) and for the bare substrate (LAO, open symbols), measured at the same magnetic fields.

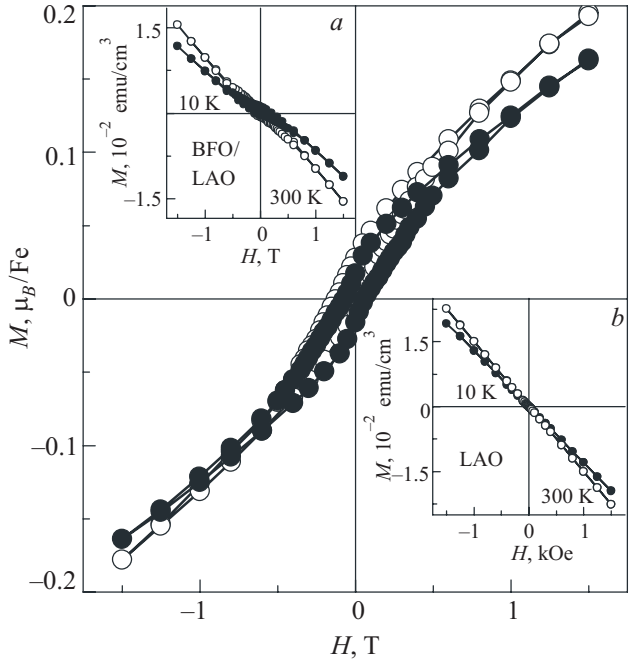

Fig. 3. In-plane magnetic hysteresis loops for the BFO film (after extracting of the substrate response), taken at room temperature (solid symbols) and 10 K (open symbols). Lines guide the eye only. Insets *a* and *b* show the raw in-plane magnetic hysteresis loops for the film with substrate (BFO/LAO) and for the bare substrate (LAO), respectively, measured at the same temperatures.

with T_N higher than a room temperature and the FM component. First statement is confirmed by the linear field dependence of magnetic moment at 300 K, which can be expressed by the empirical relation $M(300\,\mathrm{K},H) = M(300\,\mathrm{K},0)+\chi(300\,\mathrm{K})H$, where $M(300\,\mathrm{K},0)=0.009\mu_B/\mathrm{Fe}$ is a magnetic moment without an applied magnetic field and $\chi(300\,\mathrm{K}) = 0.113\mu_B/\mathrm{Fe}\cdot\mathrm{T}^{-1}$ is a magnetic susceptibility. The presence of FM phase is manifested by ZFC/FC $M(T)$ splitting, indicated by arrows.

Figure 3 presents the magnetic hysteresis loops, $M(H)$, for the BFO film at 10 K (open symbols) and 300 K (solid symbols) after an extracting of diamagnetic response from the substrate. Insets *a* and *b* show the corresponding raw $M(H)$ curves for the BFO film with substrate and for the bare LAO substrate, respectively. The $M(H)$ dependences can be treated as a superposition of the AFM (linear term) and the FM (hysteresis term with a saturation) contributions, and testify, similar to $M(T)$, to a presence of two different magnetic phases in the BFO film.

Figure 4 shows the FM contribution to the hysteresis loops for the BFO film at 10 K (open symbols) and 300 K (solid symbols) after an extracting of the AFM linear term.

Insets display the same dependencies more in detail. Analysis of the hysteresis loops reveals that a saturation magnetic moment is $M_s \simeq 0.045$ and $0.064\ \mu_B/\mathrm{Fe}$ at 300 and

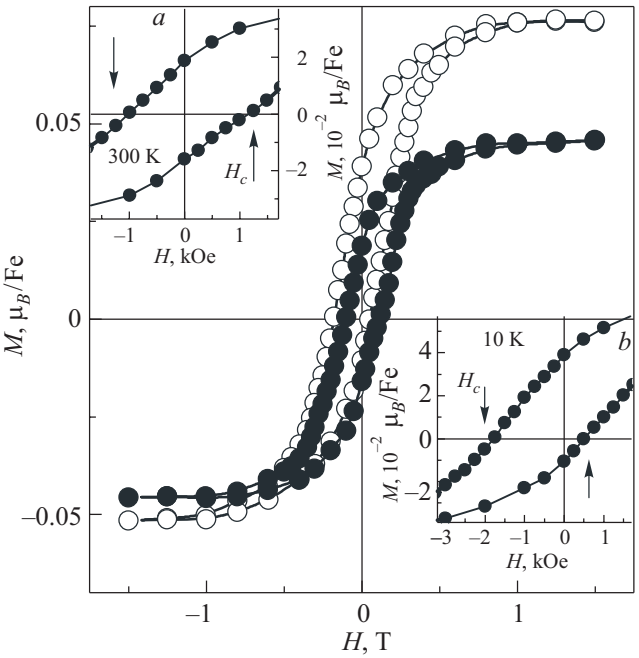

Fig. 4. FM component of the in-plane magnetic hysteresis loops for the BFO film (after extracting of the linear AFM response), taken at room temperature (solid symbols) and 10 K (open symbols). Insets *a* and *b* show the same curves in detail. Arrows indicate the coercive magnetic field. Lines guide the eye only.

10 K, respectively, which is well coincident with published values for thin films [5,6,15]. At the same time, the hysteresis loop has almost symmetric shape (within experimental error) with a coercive field of $H_c \simeq \pm 1100$ Oe, and a remanent magnetic moment $M_r \simeq \pm 0.016$ μ_B/Fe at a room temperature, which becomes greatly asymmetric with decreasing temperature: $H_c \simeq +500$ and -2500 Oe, and $M_r \simeq +0.039$ and -0.011 μ_B/Fe at 10 K. Therefore, the low-temperature hysteresis loop exhibits exchange bias field and vertical asymmetry that was observed early in the nanoscale BFO powders [11]. It is worth noting that the hysteresis loops were measured after cooling without an applied magnetic field (ZFC regime).

5. Discussion

As a rule, the weak FM response in BFO is treated as an intrinsic property of the AFM state with a specific symmetry, which is provided by the non-collinearity of magnetic sublattices (or by a spin canting) owing to the DM relativistic interaction. In this case the temperature dependence of a reduced magnetic moment for the DM-like weak FM state is proportional $\Delta M(T)/M(0) \sim T^2$, where $\Delta M(T) = M(0) - M(T)$, instead of the Bloch law $\sim T^{3/2}$, which is typical for common FMs [9]. However, Fig. 5 manifests that the experimental $\Delta M(T)$ dependences demonstrate a linear behavior rather than a parabolic law. For the sake of convenience the normalized magnetic moment was used for analysis: $\Delta M(T) = [M(0) - M(T)]/[M(0) - M(300\,\text{K})]$. Therefore, the observed FM response in our BFO film can not be treated as a result of the DM interaction only. The linear $\Delta M(T)$ dependence can be explained, assuming that an additional FM phase forms the separated FM clusters, which can be treated as an ensemble of the superparamagnetic (SPM) particles. Taking into account that the SPM state is described as a rule by Langevin function [16]: $\mathcal{L}(\alpha) = \coth(\alpha) - \alpha^{-1}$, where $\alpha = \mu_{\text{eff}} H / k_B T$, μ_{eff} is the average effective magnetic moment of the SPM particle and k_B is the Boltzmann constant, the normalized magnetic moment can be expressed as: $\Delta M(T) = [M(0) - M(0)L(\alpha)]/[M(0) - M(300\,\text{K})]$. Figure 5 shows that the experimental curves are excellently fitted by the Langevin function with variation of μ_{eff} only as a fitting parameter. For clarity, the theoretical $\Delta M(T)$ curve for $H =$ 0.1 T (solid line) is shifted along the temperature axis. The carried out fitting of the experimental $\Delta M(T)$ curves reveals that the effective magnetic moment of SPM clusters turned out to be $\mu_{\text{eff}} \simeq 1.86 \cdot 10^4$, $3.88 \cdot 10^3$ and $2.05 \cdot 10^3 \mu_B$ for an applied magnetic field $H =$ 0.1, 0.5 and 1.0 T, respectively. The observed dependence of μ_{eff} on a magnetic field is governed by the possible dipolar interaction between SPM clusters [17,18]. By taking the magnetic moment of Fe^{3+} as $\simeq 6$ μ_B/Fe and assuming a spherical shape of the SPM clusters with a volume of $\pi D^3/6$, their average diameter is estimated to be $D \simeq$ 7.3, 4.33 and 3.5 nm for a magnetic field of 0.1, 0.5 and 1.0 T, respectively. In principle, it is absolutely reasonable values and allows us to conclude that the additional FM phase exists in the film as the SPM clusters.

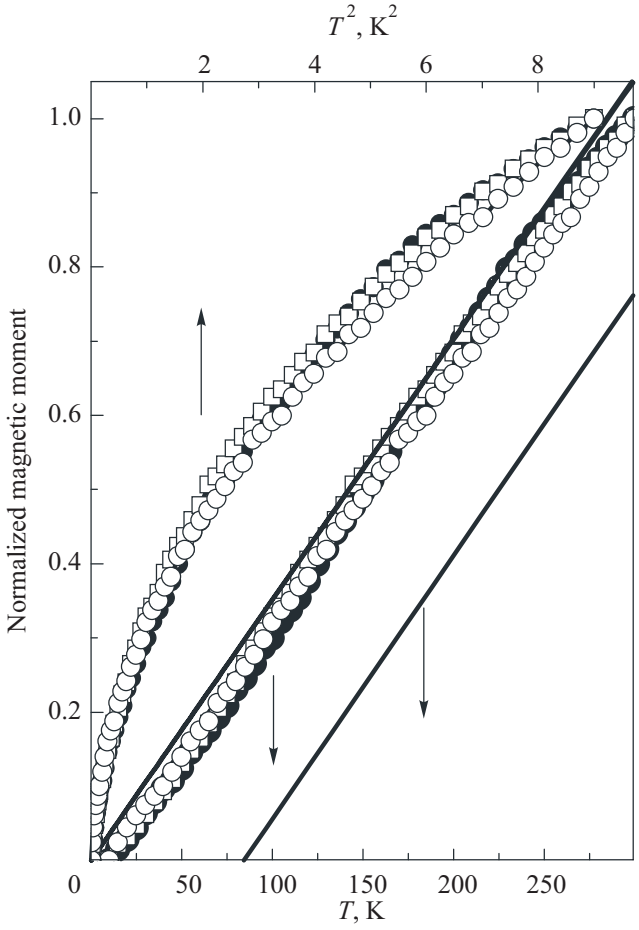

Fig. 5. Temperature-dependent normalized magnetic moment for the BFO film, taken at different applied magnetic fields: $H =$ = 0.1 (solid circles), 0.5 (open squares), and 1.0 (open circles) T. Solid line is the theoretical curve, obtained in the framework of SPM approach (described in text).

Additional peculiarity in magnetic properties of investigated films, which confirms the foregoing assumption, is connected with the asymmetric hysteresis loop, which is observed at low temperature. A shift of the hysteresis loop along the field axis is typical for the FM/AFM magnetically coupled system and called the «exchange bias» (EB) interaction. It is generally accepted that the EB, resulting from the exchange anisotropy at the FM/AFM interface, is provided by the coupling between the FM layer and the uncompensated interfacial spins in the AFM layer, the number of which determines the magnitude of exchange field (H_{EB}) [19]. Consequently, for an appearance of the EB effect the FM and AFM phases must necessary be separated to each other by interface that does not realize in a classical DM-like ferromagnet, because in this case the FM state is the *intrinsic* property of the *G*-type AFM one. On the other hand, an exchange bias has been observed in the multiferroic epitaxial heterostructures [20,21] and bilayers

[22,23], involving the common FM layers, in spite of that the *G*-type AFM state in BFO is compensated [24].

Insets in Fig. 4 manifest that the magnitude of exchange field $H_{EB} \simeq 0$ at room temperature while $H_{EB} \simeq 1000$ Oe at 10 K. It is explained by an essential transition of SPM clusters to the blocking state with decreasing temperature. Above of a certain blocking temperature (T_B) the magnetic moments of the SPM particles move freely owing to thermal fluctuations while they are transformed into the blocked state (and can be recognized as the FM phase) at $T \le T_B$. The main evidence for the presence of this transition is a significant ZFC/FC $M(T)$ splitting which does not disappear even at an applied magnetic field exceeding the coercive field. More clearly the blocked-unblocked transition is demonstrated by Fig. 6 (arrows indicate T_B). Inset presents the magnetic field dependence of the blocking temperature, which can be described by a semi-empirical expression: $T_B(H) = T_B(0)/(1+\beta H)$, where $T_B(0)$ is the blocking temperature at $H = 0$, $\beta \simeq M_s^2(0)/k_B T$ and $M_s(0)$ is a saturation magnetic moment at $H = 0$ (for a spontaneous magnetization). This expression was obtained for the interacting SPM phase, which is taken into account the strong dipolar interaction between SPM clusters [17,18,25,26].

Therefore, based on the analysis of the $M(T)$ and $M(H)$ dependences, one can conclude that the investigated BFO film can be treated as a magnetic phase separated system which consists of the G-type AFM matrix and the FM inclusions of non-DM-like origin. The formation of these inclusions is caused by the oxygen deficiency [5], which can be appeared in certain local regions of the film due to the crystal lattice imperfection or overstrain. The changing oxygen stoichiometry leads to a transformation of Fe^{3+} to Fe^{2+}, providing formation of a carrier-mediated local FM order across the Fe^{3+}–O^{2-}–Fe^{2+} chains, similar to that observed in the electron- or hole-doped manganites [27]. Consequently, in addition to the *intrinsic* DM-like weak FM state the *extrinsic* nanoscale FM clusters exist in the BFO film, which demonstrate a magnetic behavior typical for the interacting SPMs.

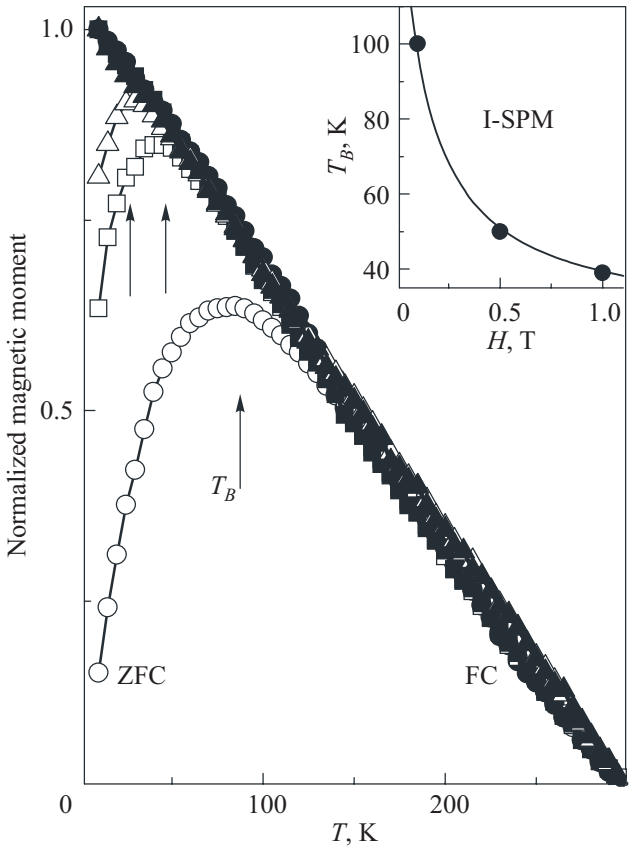

Fig. 6. Temperature dependence of the in-plane ZFC (open symbols) and FC (solid symbols) normalized magnetic moment for the BFO film, measured in an applied magnetic field of 0.1 (circles), 0.5 (squares), and 1.0 (trianles) T. Arrows indicate the blocking temperature. Lines guide the eye only. Inset shows the magnetic field dependence of the blocking temperature. Solid line is the theoretical curve, obtained on the base of model for the interacting SPM clusters (described in text).

Conclusions

$BiFeO_3$ films have been prepared by dc magnetron sputtering on $LaAlO_3$ (001) single-crystalline substrate. XRD and HREM analysis reveal that the deposition results in a highly *c*-oriented orthorhombic crystal structure. The unusual for typical DM-like ferromagnets magnetic properties, such as the linear $M(T)$ dependence, the significant ZFC/FC $M(T)$ splitting in the applied magnetic fields exceeding the coercive field and the exchange-bias effect, observed at low temperature, testify to existence of an additional *extrinsic* FM phase in the film. The magnetic behavior of this phase is well described in the framework of a phenomenological approach for the interacting SPM clusters. We argue that an appearance of the *extrinsic* FM clusters is provided by the oxygen deficiency in certain regions of the film where the FM ordering is realized through the double-exchange mechanism by Zener [27].

Acknowledgments

This work was supported by the NRF/MEST through the Quantum Photonic Science Research Center, Korea. V. Svetchnikov is grateful to the financial support of Netherlands Institute for Metal Research.

1. X. Qi, J. Dho, R. Tomov, M.G. Blamire, and J.L. MacManus-Driscoll, *Appl. Phys. Lett.* **86**, 062903 (2005).
2. W. Eerenstein, F.D. Morrison, J. Dho, M.G. Blamire, J.F. Scott, and N.D. Mathur, *Science* **307**, 1203a (2005).
3. N.A. Spaldin and M. Fiebig, *Science* **309**, 391 (2005).
4. C. Michel, J.-M. Moreau, G.D. Achenbach, R. Gerson, W.J. James, *Solid State Commun.* **7**, 701 (1969).
5. J. Wang, J.B. Neaton, H. Zheng, V. Nagarajan, S.B. Ogale, B. Liu, D. Vieland, V. Vaithyanathan, D.G. Scholm, U.V.

Waghmare, N.A. Spaldin, K.M. Rabe, M. Wittig, and R. Ramesh, *Science* **299**, 1719 (2003); *ibid.* **307**, 1203b (2005).
6. C. Ederer and N. Spaldin, *Phys. Rev.* **B71**, 069401 (2005).
7. I. Dzyaloshinskii, *J. Phys. Chem. Solids* **4**, 241 (1958).
8. T. Moria, *Phys. Rev.* **120**, 91 (1960).
9. S.V. Vansovskii, *Magnetism*, Nauka, Moscow (1973) [in Russian].
10. S.K. Singh, Y.K. Kim, H. Funakubo, and H. Ishiwara, *Appl. Phys. Lett.* **88**, 162904 (2006).
11. R. Mazumder, P.S. Devi, D. Bhattacharya, P. Choundhury, and A.S. M. Raja, *Appl. Phys. Lett.* **91**, 062510 (2007).
12. D.S. Rana, K. Takahashi, K.R. Mavani, I. Kawayama, H. Murakami, M. Tonouchi, T. Yanagida, H. Tanaka, and T. Kawai, *Phys. Rev.* **B75**, 060405(R) (2007).
13. H. Béa, M. Bibes, A. Barthelemy, A. Bouzehouane, E. Jacquet, A. Khodan, S. Fusil, F. Wyczisk, A. Forget, D. Lebeugle, D. Coloson, and M. Viret, *Appl. Phys. Lett.* **87**, 072508 (2005).
14. V.N. Varyukhin, Yu.V. Medvedev, Yu.M. Nikolaenko, A.B. Mukhin, B.V. Belyaev, V.A. Gritskikh, I.V. Zhikharev, S.V. Kara-Murza, N.V. Korchikova, and A.A. Tikhii, *Technical Phys. Lett*. **35**, 937 (2009).
15. T. Sun, Z. Pan, V.P. Dravid, Z. Wang, M.-F. Yu, and J. Wang, *Appl. Phys. Lett.* **89**, 163117 (2006).
16. C.L. Cullity, *Introduction to Magnetic Materials*, Addison-Wesley, New York (1972).
17. V.G. Prokhorov, G.G. Kaminsky, V.A. Komashko, Y.P. Lee, S.Y. Park, Y.H. Hyun, J.B. Kim, J.S. Park, V.L. Svetchnikov, V.P. Pashchenko, and V.A. Khokhlov, *Fiz. Nizk. Temp.* **33**, 889 (2007) [*Low Temp. Phys.* **33**, 678 (2007)].
18. V.G. Prokhorov, Y.H. Hyun, J.S. Park, J.B. Kim, G.H. Kim, Y.S. Lee, Y.P. Lee, and V.L. Svetchnikov, *J. Appl. Phys.* **104**, 103901 (2008).
19. J. Nagués and I.K. Schuller, *J. Magn. Magn. Mater.* **192**, 203 (1999).
20. V. Laukhin, V. Skumryev, X. Marti, D. Hrabovsky, F. Sánchez, M.V. García-Cuenca, C. Ferrater, M. Valera, U. Lüders, J.F. Bobo, and J. Fontcuberta, *Phys. Rev. Lett.* **97**, 227201 (2006).
21. L.W. Martin, Y.-H. Chu, M.B. Holcomb, M. Huijben, P. Yu, S.-J. Han, D. Lee, S.X. Wang, and R. Ramesh, *Nano Lett*. **8**, 2050 (2008).
22. J. Dho and M.G. Blamier, *J. Appl. Phys.* **106**, 073914 (2009).
23. H. Béa, M. Bibes, F. Ott, B. Dupé, X.-H. Zhu, S. Petit, S. Fusil, C. Deranlot, K. Bouzehouane, and A. Barthélémy, *Phys. Rev. Lett.* **100**, 017204 (2008).
24. S. Dong, K. Yamauchi, S. Yunoki, R. Yu, S. Liang, A. Moreo, J.-M. Liu, S. Picozzi, and E. Dagotto, *Phys. Rev. Lett.* **103**, 127201 (2009).
25. P. Allia, M. Coisson, P. Tiberto, F. Vinai, M. Knobel, M.A. Novak, and W.C. Nunes, *Phys. Rev.* **B64**, 144420 (2001).
26. O. Margeat, M. Tran, M. Spasova, and M. Farle, *Phys. Rev.* **B75**, 134410 (2007).
27. For the review, see*: Colossal Magnetoresistance, Charge Ordering and Related Properties of Manganese Oxides*, C.N.R. Rao and B. Raveau (eds.), World Scientific, Singapore (1998); *Colossal Magnetoresistance Oxides*, Y. Tokura (ed.), Gordon and Breach, London (1999); E. Dagotto, T. Hotta, and A. Moreo, *Phys. Rep*. **344**, 1 (2001).